ELSEVIER

Deep-Sea Research II 53 (2006) 31–41

DEEP-SEA RESEARCH
PART II

www.elsevier.com/locate/dsr2

Decadal variability of wind-energy input to the world ocean

Rui Xin Huang[a,b,*], Wei Wang[b], Ling Ling Liu[b]

[a]*Department of Physical Oceanography, Woods Hole Oceanographic Institution, Woods Hole, MA 02543, USA*
[b]*Physical Oceanography Lab, Ocean University of China, Qingdao 266003, Shandong, PR China*

Received 4 April 2005; received in revised form 18 August 2005; accepted 4 November 2005

Abstract

Wind-stress energy input to the oceans is the most important source of mechanical energy in maintaining the oceanic general circulation. Previous studies indicate that wind-energy input to the Ekman layer and surface waves has varied greatly over the past 50 years. In this study, wind-energy input to surface current and surface geostrophic current was calculated as the scalar product of wind stress and surface current and surface geostrophic current. The surface geostrophic current was calculated in two ways: the surface geostrophic velocity was diagnosed from the TOPEX/POSEIDON altimeter data between 1993 and 2003, and calculated from the sea-surface height of the numerical model. The surface velocity was obtained from a numerical model. Estimate of wind-energy input based on altimetric data averaged over 1993–2003 is 0.84 TW (1 TW = 10^{12} W), excluding the equatorial band (within $\pm 3^{\circ}$ of the equator). Estimate of the wind-energy input to the surface geostrophic current based on the numerical model is 0.87 TW averaged from 1993 to 2003, and wind-energy input to the surface current for the same period is 1.16 TW. This input is primarily concentrated over the Southern Ocean and the equatorial region ($20^{\circ}S - 20^{\circ}N$). This energy varied greatly on interannual and decadal time scales, and it increased 12% over the past 25 years, and the interannual variability mainly occurs in the latitude band of $40^{\circ}S - 60^{\circ}S$ and the equatorial region.

Keywords: Wind energy; Decadal variability; Geostrophic current

1. Introduction

A new paradigm of the oceanic general circulation is emerging. Although the ocean receives a huge amount of thermal energy, it cannot convert such thermal energy into mechanical energy very efficiently because the ocean is heated and cooled from the same geopotential level, the upper surface. The inability of thermal forcing in driving the oceanic circulation can be traced back to the classical theorem postulated by Sandström (1908, 1916), and it has been discussed in many recent studies (e.g. Huang, 1999; Paparella and Young, 2002). Recently, Wang and Huang (2005) have demonstrated the basic idea through laboratory experiments.

Therefore, the oceanic circulation requires external sources of mechanical energy to balance the loss of mechanical energy due to friction and dissipation. As a result, for a quasi-steady circulation, the distribution of mechanical energy sources and sinks dedicates the strength of circulation and its variability.

Historically, the old wisdom was that thermohaline circulation is driven by surface thermohaline forces. For a long time, nobody paid much attention

*Corresponding author.

0967-0645/$ - see front matter © 2006 Elsevier Ltd. All rights reserved.
doi:10.1016/j.dsr2.2005.11.001

to the connection between tidal dissipation and thermohaline circulation. It is only during the past 10 years that the oceanic community has realized the important role of tidal dissipation in driving diapycnal mixing in the deep ocean. The recent estimate of tidal dissipation in the open ocean is 0.7–0.9 TW (Munk and Wunsch, 1998). Due to the inspiration by Munk and his colleagues, tidal dissipation has become one of the most active research frontiers in recent years, with large-scale field programs being carried out and many papers reporting observational, theoretical, and numerical results. However, tidal dissipation may not be the most important problem for oceanic general circulation and climate due to the following reasons.

First, wind-stress energy input into the open ocean is at least 50 times larger than that due to tidal dissipation (Huang, 2004). Wind-stress energy input to the surface geostrophic current is estimated as 0.88 TW (Wunsch, 1998). Wind-stress energy input to the surface waves is estimated as 60 TW (Wang and Huang, 2004a); wind-stress energy input to the Ekman layer is estimated as 0.5–0.7 TW over the near-inertial frequency (Alford, 2003; Watanabe and Hibiya, 2002), and the energy input over the sub-inertial range is about 2.4 TW (Wang and Huang, 2004b). A major part of wind-energy input to surface waves and Ekman layer may be lost in the upper ocean; however, even if a small portion of this energy is transported into the sub-surface ocean, it will play a major role in regulating the oceanic general circulation.

Second, in the open ocean, tidal-driven mixing is mostly bottom trapped. On the other hand, wind-stress energy input plays a dominating role in setting up the density structure and circulation in the upper 500–1000 m in the open ocean. Thus, wind-stress energy plays a much more important role than tidal mixing for many applications that are intimately related to the circulation in the top 1000 m, including climate variability, ecology, fishery, and environmental studies.

Third, wind-stress energy input varies greatly over broad time scales, from interannual to millennial. On the other hand, tidal dissipation does not vary much for time scales shorter than centennial. Noticeable changes in tidal dissipation take place over long geological time scales. For example, during the Last Glacial Maximum, tidal dissipation rate was substantially higher than the present-day rate (Egbert et al., 2004). As Wang and Huang (2004a, b) showed, wind-stress energy input to surface waves and Ekman layer has increased nearly 25% over the past 50 years. Thus, it is postulated that mixing in the upper ocean should vary accordingly. As a result, the oceanic general circulation should vary in response.

Since wind-stress energy input to surface waves and Ekman layer has varied so much over the past 50 years, similar changes in wind-energy input to the surface geostrophic current are expected. The variability of the latter turns out to be more important for the study of climate variability. Although deep mixing driven by tidal dissipation in the open ocean is a vital component in maintaining the meridional overturning circulation in the ocean, wind-stress energy input into the surface geostrophic currents in the Southern Ocean is another very important contributor. Toggweiler and Samuels (1995, 1998) have demonstrated that wind stress plays a dominating role in setting up the meridional overturning circulation observed in the world oceans. Even if the vertical mixing coefficient was set to zero, there is still a meridional overturning circulation rather similar to the observed circulation in the world oceans. (Note that due to the artificial diapycnal mixing in a z-coordinates model, Toggweiler and Samuels's numerical experiment should be interpreted with caution; nevertheless, their results indicate an important factor that wind stress is the dominating controller in setting up the meridional overturning circulation under the modern climate.)

The main goal of this study is to estimate the interannual variability of wind-energy input to surface geostrophic current over the world oceans. Early attempt to estimate wind-energy input based on ship-drift data was made by Oort et al. (1994). However, their estimate turns out to be inaccurate due to the limitation of ship-drift data. A more accurate estimate of surface geostrophic currents can be obtained from satellite data. Paralleling the study by Wunsch (1998), wind-energy input to the surface geostrophic current is calculated as the scalar product of wind stress and surface velocity:

$$w = \langle \vec{\tau} \cdot \vec{u}_g \rangle, \tag{1}$$

where $\vec{\tau}$ is the wind stress, $\vec{u}_g = (u_g, v_g)$ the surface geostrophic velocity, and the bracket denotes a time average. The wind generates a multiple of small-scale oceanic motions: ripples, gravity waves, Langmuir cells, turbulent mixing motions, Ekman-like flow, etc. (Lueck and Reid, 1984). Use of Eq. (1) assumes that all such small-scale motions are

dissipated within the surface-mixed layer and do not directly produce any motions included in the general circulation (Wunsch, 1998).

Wind-stress energy input to surface geostrophic current is closely related to gravitational potential energy in the ocean, and this energy supports the Ekman upwelling of cold and dense water in the sub-polar oceans and strong upwelling in the Antarctic Circumpolar Current (ACC) and coastal upwelling zones (Gill et al., 1974; Wang and Huang, 2004b).

Two kinds of wind-stress data sets were used in this study. The wind-stress data set of the daily mean NCEP–NCAR Reanalysis I was taken from the website (http://iridl.ldeo.columbia.edu/SOURCES). This data set covers the period from 1948 to 2003 and has a zonally uniform spacing of 1.875° and a meridionally nonuniform spacing that varies from 1.89° at the poles to 2.1° near the equator. The daily mean ECMWF ERA-40 Reanalysis data set was taken form the website (http://data.ecmwf.int/data/d/era40_daily). This data set covers the period form 1958 to 2001 and has a spatial resolution of 2.5°, both in zonal and meridional directions.

The surface geostrophic velocity can be calculated in two ways. First, it can be diagnosed from sea-surface height obtained from satellite data, assuming geostrophy. Second, it can be obtained from the sea-surface height of an oceanic general circulation model.

2. Estimation of energy input based on altimetric data

In this study, we use the TOPEX/POSEIDON altimeter data at the crossover point of the orbits provided by AVISO. It has an 11-year long time series with a basic sampling rate of 10 days. This data set is from January 1, 1993 to December 10, 2003 (cycle 11–414), which covers 66°S − 66°N with a sample matrix of 127 × 116. The zonal resolution is 2.8° and the meridional resolution is 0.02° at the northern and southern boundaries, and 3° near the equator. In this study, the altimetric data were used in forms of 10-day average field, H, and the geoid undulation at each crossover point, $\eta(x, y)$, was computed from EGM96 solution (Lemoine et al., 1997). The dynamic topography field, $\phi = H - \eta$, was interpolated onto a regular grid with a uniform horizontal resolution of 1° × 1°. Therefore, the 10-day mean geostrophic velocity, $\vec{u}_g$, can be estimated using the geostrophic relation

$$\vec{u}_g = \frac{\vec{g}}{f} \times \nabla\phi, \tag{2}$$

where $\vec{g}$ is the gravitational acceleration and f the Coriolis parameter.

The annual mean energy-input rate can thus be calculated by

$$\bar{W} = \frac{1}{n}\sum_{i}^{n} \iint \vec{\tau}(x, y) \cdot \vec{u}_g(x, y)\, \mathrm{d}x\, \mathrm{d}y,$$

where n is the number of cycles of the specific year. For the purpose of estimating the total work done by wind stress on geostrophic current, we did not separate the wind stress and the geostrophic current into mean and anomaly. Since surface height signals obtained from satellite altimetry are in forms of average over 10-day period, the wind-stress data, $\vec{\tau}$, were also averaged over the same 10-day period and were interpolated onto the regular grid of 1° × 1°.

Using wind stress from the NCEP–NCAR Reanalysis data set, the global-mean rate of mechanical energy input is 2.7 mW/m^2, with the global sum of 0.84 TW, averaged over the period of 1993–2003. Note that the trajectories of the satellite altimeter do not cover latitudes higher than 66°. Furthermore, energy input for the equatorial band (within ±3° of the equator) is omitted because geostrophic approximation is invalid near the equator. Thus, this value of 0.84 TW underestimates the total energy flux. The mean energy input averaged from 1993 to 1996 is 0.81 TW, which is slightly smaller than the previous estimate value of 0.88 TW averaged over the same period by Wunsch (1998).

The variability of the work done by wind on the geostrophic current is shown in Fig. 1 and the mean distribution is shown in Fig. 2. The mechanical energy input through geostrophic current varies greatly with time, and the amplitude is about 20% of the mean value over the past decade.

As discussed by Scott (1998, 1999), the uncertainty in the sea-surface height arises from several sources, but the dominant uncertainty in the ocean dynamic topographic is mainly associated with the geoid height field, which can cause large errors in the Northern Hemisphere. However, for the world ocean, the error in estimating $\bar{W}$ is greatly reduced to 6.4% (Table 4.2, Scott, 1998). In his studies, Scott (1998, 1999) used the first 4 years of T/P altimeter data set (TP cycles 5–154) and the geoid

undulation was estimated by the JGM-3 gravity model. The wind stress was NCEP/NCAR Reanalysis I data set. Scott found that the estimate of the geoid gradient error tends to decrease as the area of integration becomes larger, which demonstrates that geoid errors are less correlated with the (estimated) wind-stress fields than the surface current. As a result, as one increases the area of integration, the power input to the surface currents increases more rapidly than the variance of the power input estimated from the full geoid error covariance matrix.

The relatively sparse crossover points of altimetric data at low latitude are unable to distinguish the various narrow and counter flow, and the inability to estimate the geostrophic current at the equatorial band will also cause errors in estimating $\bar{W}$. In studying the decadal variability of the wind work input to geostrophic current, the available 11-year long data set is obviously insufficient. To overcome these difficulties, we can use velocity field obtained from a numerical model, although errors may exist in model results.

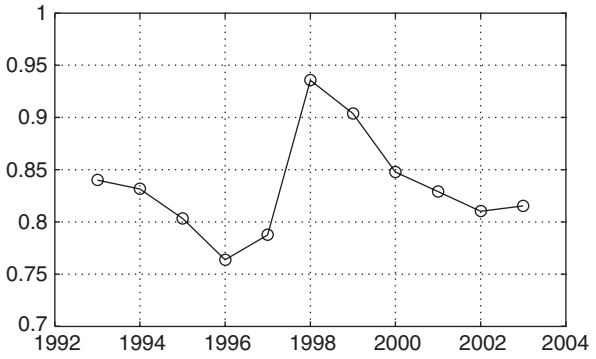

Fig. 1. Annual mean energy input from NCEP/NCAR wind stress to surface geostrophic current diagnosed from altimetric data, in units of TW.

3. Estimation of energy input based on a numerical model

Wind stress applied to the sea surface drives both surface currents and waves. Ignoring the high-frequency component associated with wave motion, the surface velocity can be separated into two components:

$$\vec{u}_0 = \vec{u}_{0,G} + \vec{u}_{0,AG}, \tag{3}$$

i.e. the geostrophic current and the ageostrophic current (the surface Ekman transport). The velocity field in the upper ocean obtained from a numerical model is a combination of these two components and there is no easy way to separate them. According to the classical theory of Ekman layer, the vertically integrated volume flux associated with the ageostrophic flow is perpendicular to the surface wind stress. As a result, if the surface layer is thick enough (much larger than the Ekman depth), errors in wind-energy contribution due to the ageostrophic current will be maximally reduced. The spatial averaged thickness of the first layer in our numerical model was about 30 m; it varied with the buoyancy forcing from place to place. As a result, the contribution of the wind-energy input to the ageostrophic current is not negligible. Another way of calculating the geostrophic current is to infer it from sea-surface height obtained from the numerical model. However, geostrophy does not

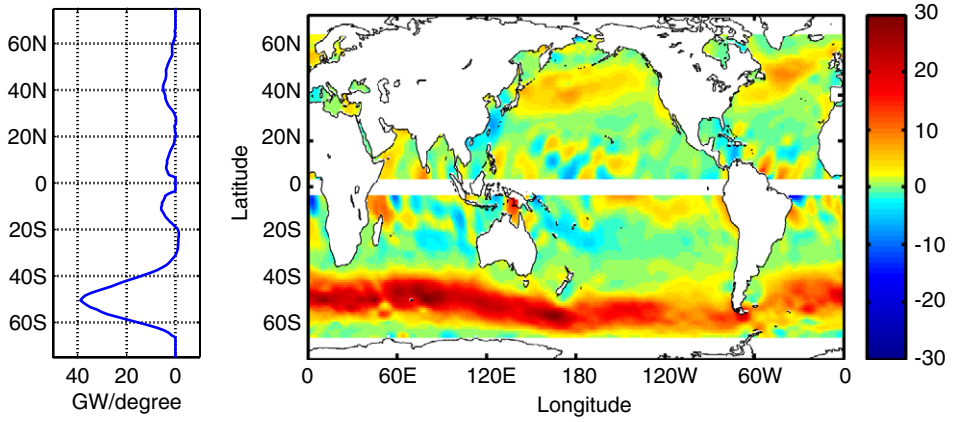

Fig. 2. The horizontal distribution of the wind-energy input to the geostrophic current estimated with altimetric data averaged over the period of 1993–2003 (right panel, in units of mW/m^2), and the meridional distribution of the zonal integrated results (left panel).

apply to the equatorial band, so this approach does not apply to this area.

The NCEP–NCAR (or ECMWF ERA-40) daily wind-stress data set interpolated onto regular grid of $1^\circ \times 1^\circ$ was used as surface-stress forcing in the numerical model. The surface velocity field and the surface-height field were obtained, using the Hallberg Isopycnal Model (HIM; Hallberg, 1997). In the model, the temporal resolution is 20 min, the horizontal resolution is $1^\circ \times 1^\circ$. The model has 19 layers in the vertical direction, including a Kraus-Turner (1967) bulk mixed layer and a layer underneath that plays the role as a buffer layer between the mixed layer and the layers below. The model domain covers the ocean from 72°S to 72°N. The Levitus annual mean temperature and salinity fields were interpolated onto the model grid as initializing fields and the restoring fields in the uppermost level.

The model was first run with NCEP–NCAR monthly mean wind stress of 1948 for 100 years to reach a quasi-equilibrium. Afterward, the model was restarted from this quasi-equilibrium state and run with the NCEP–NCAR daily mean wind stress of 1948 for 50 years to achieve a second quasi-steady state. Finally, the model was restarted from this second quasi-equilibrium and run under the NCEP–NCAR daily mean wind stress from 1948 to 2003. Daily mean surface velocity from this final run was used to calculate wind-energy input. For the numerical experiment with ECMWF ERA-40, wind stress followed the same procedure, except a slightly different starting (ending) time at 1958 (2001) was used. Unless specified, all results in the following studies are attributing to the case with NCEP–NCAR wind stress.

The annual wind-energy input to the oceanic general circulation is defined as the average of the energy input, based on the daily mean value, i.e.

$$W = \frac{1}{N}\sum_{i}^{N} W_i, \tag{4}$$

where N is the number of days of a specific year and W_i the wind-energy input for the ith day in this year.

The horizontal distribution of wind-energy input to the surface current, $\vec{u}_0$, averaged over the past 56 years is shown in Fig. 3. Note that the wind-energy input is primarily due to work by the zonal wind in the Southern Ocean, the equatorial region (from 20°S to 20°N) and (to a lesser degree) the Kuroshio and Gulf Stream regions. From the meridional distribution of the zonal integrated results (left panel, Fig. 3), it is readily seen that most of the energy input is accumulated in the ACC region and the equatorial region. The contribution due to the meridional wind-stress component is much smaller than the zonal one, with exceptions along the western/eastern boundaries of the basins where wind-energy input is strong due to comparatively strong along-shore wind. Note that, although the latitudinal band used in our numerical model is larger than that used in the calculation based on altimeter data, it does not cover the globe and leaves out a small part of the Southern Ocean and the Arctic. Thus, the value calculated from our model may slightly underestimate the total wind-energy input.

The annual mean rate of wind-energy input to the surface current, $\vec{u}_0$, varied greatly over the past 56

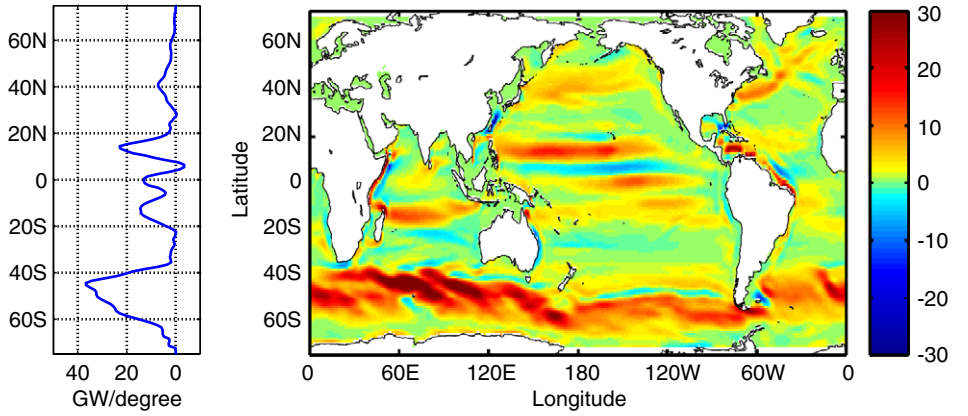

Fig. 3. Wind-energy input to the surface geostrophic current calculated from the numerical model averaged over a period from 1948 to 2003 (right panel, in units of mW/m^2), and the meridional distribution of the zonal integrated results (left panel).

years, and the results that correspond to the wind-stress data set of ECMWF ERA-40 for time period of 1958–2001 showed a very similar pattern (Fig. 4). For better comparison, the data shown in Fig. 4 were normalized by their individual mean. The mean energy-input rate due to wind stress of NCEP–NCAR is 1.10 and 1.14 TW averaged over the period of 1958–2001 and 1993–1996, respectively. The mean energy input due to wind stress of ECMWF ERA-40 is 1.20 and 1.21 TW averaged over the same period mentioned above. For time period of 1993–1996, these two results were comparable with the estimated value of 1.0 TW by Wunsch (1998). It is clearly seen that the results from NCEP/NCAR wind stress and ECMWF ERA-40 wind stress are quite close to each other,

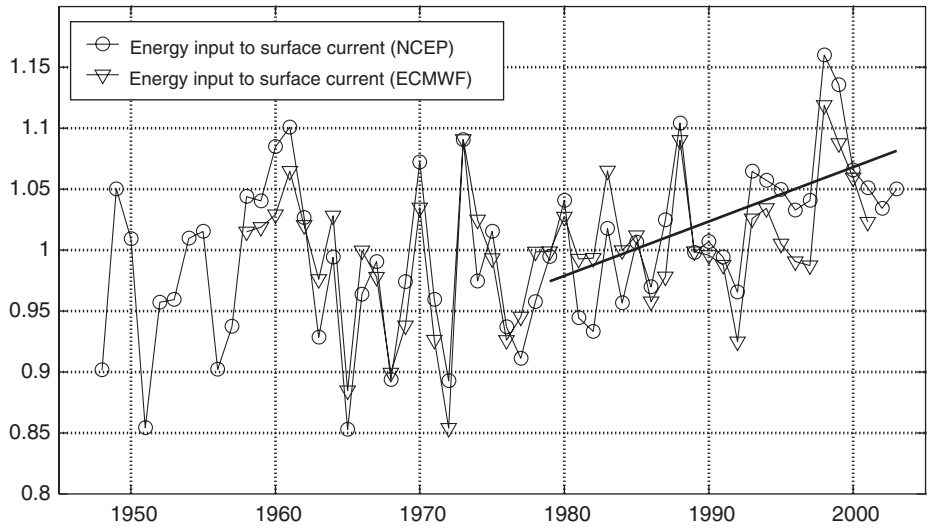

Fig. 4. Comparison of the normalized annual mean wind-energy input to surface current diagnosed from NCEP/NCAR wind-stress data set and the ECMWF ERA-40 wind-stress data set, and the black straight line is the best fitting of the NCEP–NCAR results over the period of 1979–2003.

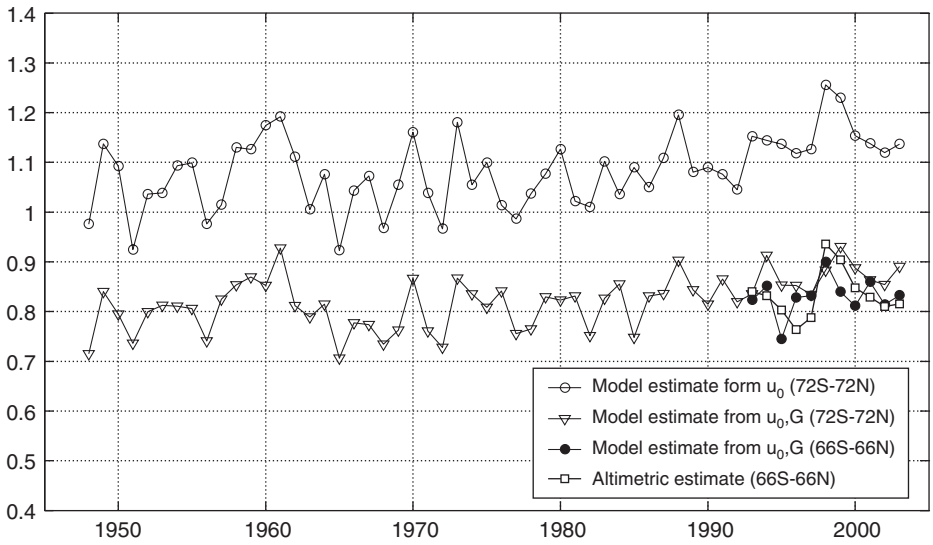

Fig. 5. Annual mean wind-energy input to surface current (base on NCEP/NACA wind stress) diagnosed from numerical model (72°S – 72°N) (open cycle), the results diagnosed form model geostrophic current in region 72°S – 72°N (open triangle) and in region 66°S – 66°N (solid cycle), and the results from altimetric data (solid square), in units of TW.

with less than 10% in the mean value and almost the same time-evolution profile over the past 40 years.

Fig. 5 shows the comparison of the numerical model results and that diagnosed from satellite data. Also shown in Fig. 5 is the comparison of wind-energy input to the surface current, $\vec{u}_0$ and wind-energy input to the surface geostrophic current, $\vec{u}_{0,G}$. For time period of 1993–2003 when altimetric data are available, mean wind-energy-input rate diagnosed from the altimetric data is 0.84 TW for the area between 66°S and 66°N and excluding the equatorial band. Mean wind-energy-input rate diagnosed from sea-surface height of the numerical model for the same area and time period is 0.83 TW, which can be considered identical to the result of that diagnosed from the altimetric data. Furthermore, interannual variability diagnosed from these two approaches is quite similar. For the area between 72°S and 72°N and excluding the equator band, wind-energy-input rate diagnosed from sea-surface height of the numerical model averaged over the same time period is 0.87 TW, increased about 5% due to the contribution of the additional 12° area at high latitudes, where there is no ice coverage in the numerical model, in contrast to the altimeter data. The mean wind-energy input to the surface current, $\vec{u}_0$, in the area between 72°S and 72°N for the same time period is 1.16 TW, which implies that the contribution of ageostrophic current, $\vec{u}_{0,AG}$, of the numerical model to the wind-energy input is about 0.3 TW.

For time period of 1948–2003, the interannual variability of the wind-energy input to the surface current and to the geostrophic current is also quite consistent with each other (Fig. 5). Therefore, the discussions below will be focused on the wind-energy input to surface current.

It was suggested by Kistler et al. (2001) that the climatology based on the years 1979–present is most reliable due to the introduction of satellite data in 1979. Also shown in Fig. 4 is that the interannual variability of the wind-energy input to surface current before 1979 changes greatly and does not show an obvious trend. However, the amplitude of the interannual variability after 1979 is largely reduced and shows an obvious trend as illustrated by the black straight line in Fig. 4, which has a slope of about 5×10^{-3} that corresponds to a 12% increase of wind-energy input to surface current over the past 25 years. The horizontal distribution of the variability can be clearly seen from the standard deviation of the wind-energy input for time period from 1979 to 2003 (Fig. 6). The variability is mainly distributed in the Southern Ocean and in the equatorial region. Although both the equatorial region and the Southern Ocean are regions of strong wind-energy input and strong interannual variability of wind-energy input, the trend of energy input for these two regions are quite different (Fig. 7). In fact, most of the large interannual variability in the total amount of energy input shown in Fig. 4 during time period from 1948 to 1978 can be attributed to the variations in the equatorial region. In contrast, the wind-energy input to the equatorial region only slightly increased from 1979 to 2003, with a slope of about $\frac{1}{3}$ of that in the ACC region for the same period and the amplitude of the interannual variability greatly reduced. The different slopes of the energy input to the ACC region and to the equatorial region for

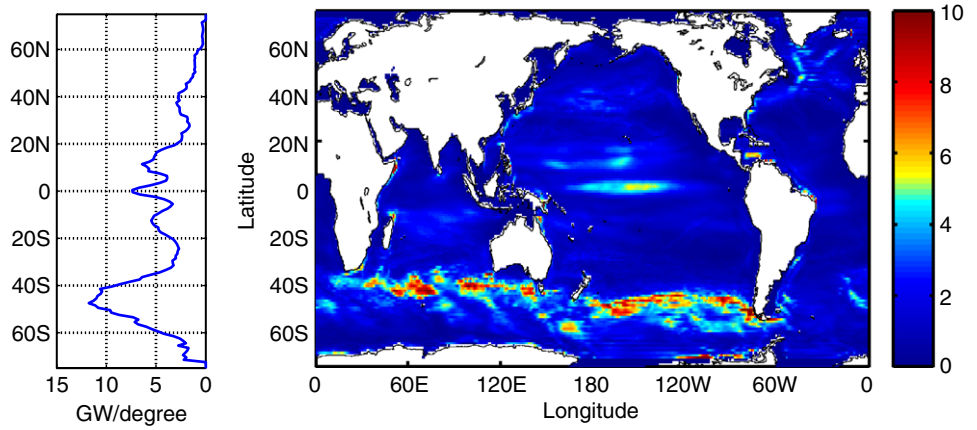

Fig. 6. Standard deviation of the wind-energy input to surface current (right panel, in units of mW/m^2) and the meridional distribution of the standard deviation variance (left panel).

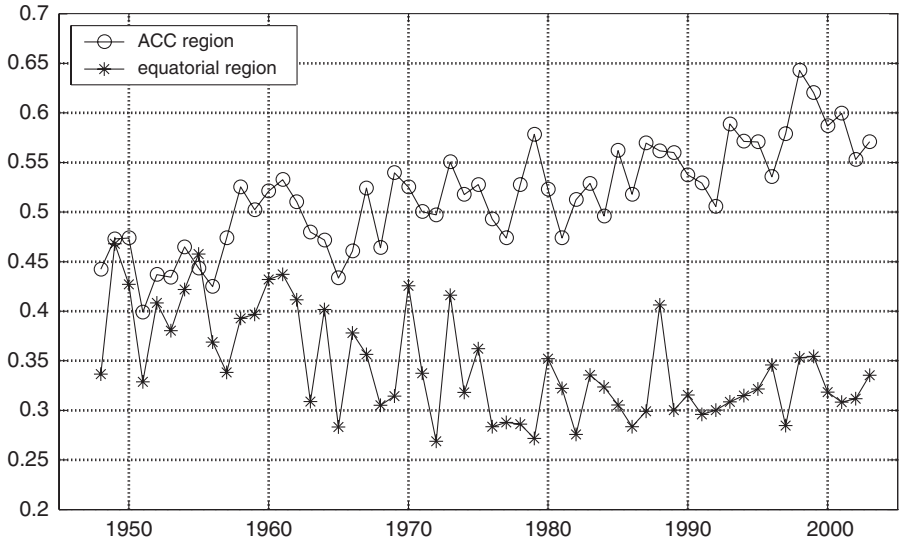

Fig. 7. Annual mean wind-energy input to the sea-surface current in equatorial region and ACC region from 1948 to 2003, in units of TW.

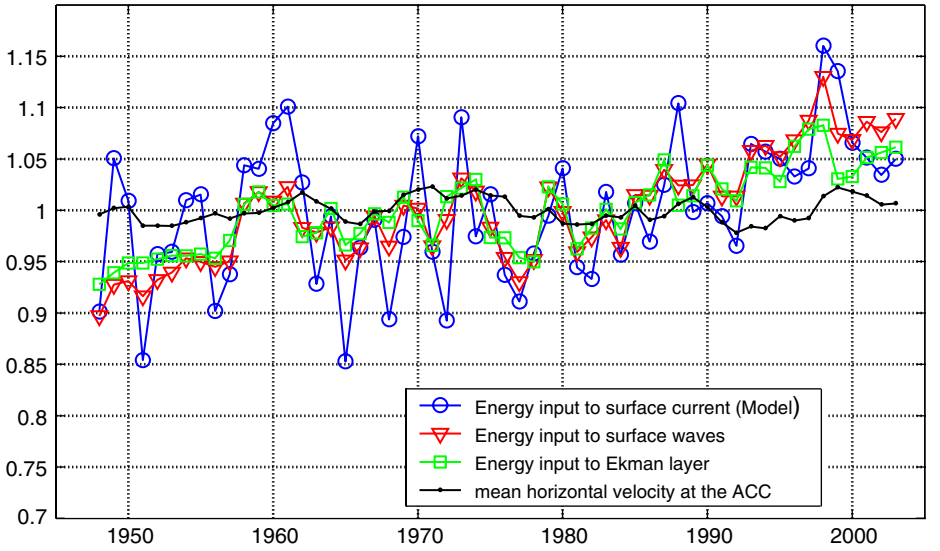

Fig. 8. The time evolution of the normalized wind-energy input through surface currents (circle), surface waves (triangle), and Ekman layer (square) and the variability of the mean horizontal velocity at ACC region (dot).

the time period from 1979 to 2003 result in a continuous change in the partition of wind-energy input to the world oceans. Thus, at the present time, the ACC region becomes a more and more dominant site for wind-energy input to the surface current in the world oceans, although the annual mean flow rate of the ACC almost not changed (Fig. 8). Since wind-energy input may be directly related to the baroclinic instability activity in the ocean, the global distribution of baroclinic eddy activity must vary greatly over the past 25 years.

It is quite interesting to compare the trend of wind-energy input to surface currents, with wind-energy input to surface waves (Wang and Huang, 2004a) and to Ekman layer (Wang and Huang, 2004b). Since the mean values of these energy inputs differ greatly, these three data sets were normalized by the individual mean over the period from 1948 to 2003 (Fig. 8). It is readily seen that the trends of all

three wind-energy inputs are rather similar, especially for time period from 1979 to 2003, i.e. there is a similar trend of an increasing energy input from wind stress over the past 25 years, which is closely related to the general trend of wind-stress changes over the same period. A typical scenario of global warming is a reduced equator-to-pole temperature gradient. As a result, wind stress might be reduced. However, wind-stress data set from NCEP–NCAR indicates that over the past 50 years, changes in wind stress is characterized by a noticeable intensification of the southern westerly over the ACC region and a weakening of the easterly over the equatorial region (Fig. 9). Wind-stress variability in the Southern Ocean may be closely related to the Antarctic Oscillation and the global environmental change, especially the intensification of the ozone hole in the South Pole. Ozone depletion can induce cooling in the lower stratosphere, making the Antarctic vortex tighter and more intense (Mahlman et al., 1994). The detailed mechanism of the wind-stress change over the global oceans remains to be explored. For oceanic circulation study, however, the most crucial challenge is what is the dynamical impact of such remarkable changes in the amplitude and distribution of wind-stress energy input to the world oceans.

4. Conclusions

Wind-energy input to surface geostrophic current in the world oceans was calculated through two approaches. The first approach was based on the TOPEX/POSEIDON altimeter data on crossover points of the orbits and 10-day mean wind stress from the NCEP–NCAR Reanalysis data set; for the past 11 years (1993–2003), the rate of work input through geostrophic flow was estimated as 0.84 TW. The second approach was based on the surface geostrophic current calculated form the sea-surface height and surface velocity field obtained from a numerical model (HIM) and daily mean wind stress

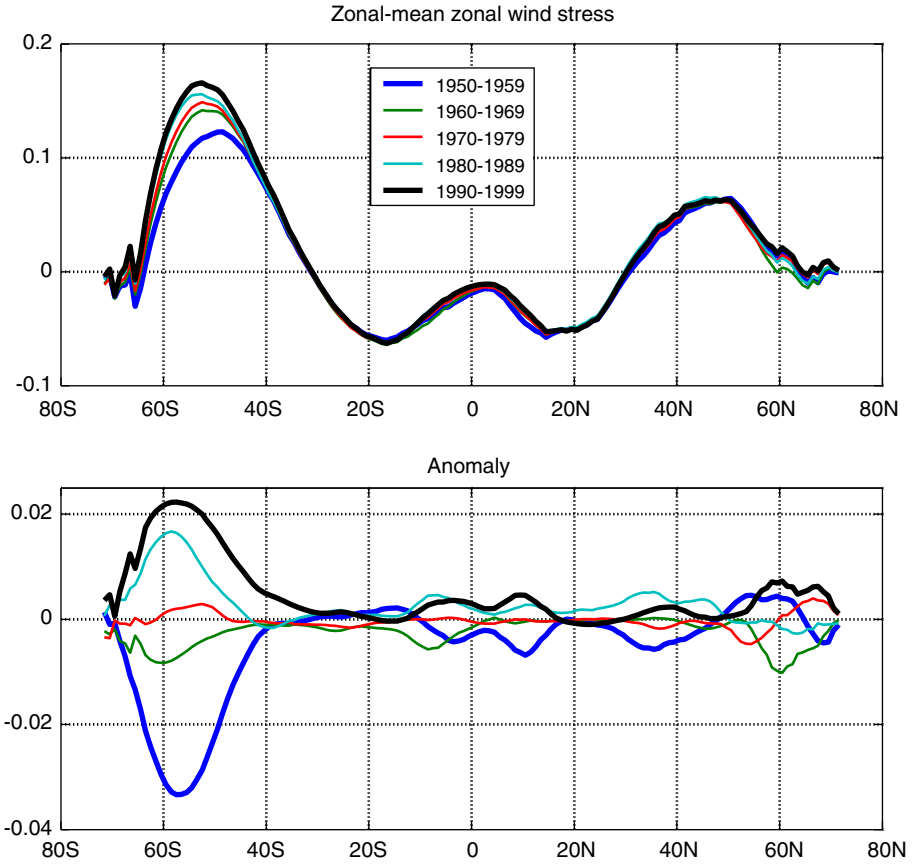

Fig. 9. Meridional distribution of the decadal-mean zonal-mean zonal wind stress (upper penal), and the anomaly to the long-term mean (lower penal), in units of Pa.

from NCEP–NCAR; the rate of wind-energy input to surface geostrophic current was estimated as 0.87 TW, and wind-energy input to the surface currents was estimated as 1.16 TW, averaged over the period from 1993 to 2003.

Mechanical energy input from wind stress to surface geostrophic flow is one of the important sources for the maintenance of a quasi-steady circulation in the world ocean. Although this contribution is much smaller than that through surface waves and Ekman layer, it is directly converted into the kinetic energy and gravitational potential energy of the mean state (Fofonoff, 1981; Wang and Huang, 2004b).

Although diapycnal mixing in the deep ocean plays a vital role in setting up the stratification in the world ocean, wind-stress energy input to the ACC is a more important controller of the meridional overturning circulation in the world oceans under the current climate condition. Therefore, great changes in this energy source, including its magnitude and spatial distribution, should affect the global circulation in many ways. For example, a 15% increase in energy input to the ACC over the past 25 years should induce remarkable changes, including the intensification of barotropic and baroclinic eddy activity, a stronger northward Ekman mass transport, which may further enhance the meridional overturning circulation in the world ocean, in particular that in the Atlantic sector. In summary, changes in wind-energy input may induce great changes in the wind-driven and thermohaline circulation in the world oceans, which should be carefully examined in further study.

Acknowledgments

CLS AVISO Operations Center generously supplied us with the TOPEX/POSEIDON altimeter data. RXH was supported by the National Oceanic and Atmospheric Administration through CICOR Cooperative Agreement NA17RJ1223 and the National Aero-Space Administration through Contract No. 1229833 (NRA-00-OES-05). WW and LLL were supported by the National Nature Science Foundation of China through grant 40476010 and Research Fund for the Doctoral Program of Higher Education through grant 20030423011. Reviews' comments helped to clean up the presentation.

References

Alford, M.H., 2003. Improved global maps and 54-year history of wind-work done on the ocean inertial motions. Geophysical Research Letters 30, 1424.

Egbert, G.D., Ray, R.D., Bills, G., 2004. Numerical modeling of the global semidiurnal tide in the present day and in the Last Glacial Maximum. Journal of Geophysical Research 109, C3003.

Fofonoff, N.P., 1981. The Gulf Stream system. In: Warren, B.A., Wunsch, C. (Eds.), Evolution of Physical Oceanography. The MIT Press, Cambridge, MA, pp. 112–139.

Gill, A.E., Green, J.S.A., Simmons, A.J., 1974. Energy partition in the large-scale ocean circulation and the production of mid-ocean eddies. Deep-Sea Research 21, 499–528.

Hallberg, R., 1997. Stable split time stepping schemes for large-scale ocean modeling. Journal of Computational Physics 135, 54–65.

Huang, R.X., 1999. Mixing and energetics of the thermohaline circulation. Journal of Physical Oceanography 29, 727–746.

Huang, R.X., 2004. Ocean, energy flow. In: Cleveland, C.J. (Ed.), Encyclopedia of Energy, vol. 4. Elsevier, Oxford, pp. 497–509.

Kistler, R., Kalnay, E., Collins, W., Saha, S., White, G., Woollen, J., Chenlliah, M., Ebisuzaki, W., Kanamitsu, M., Kousky, V., Dool, H., Fiorino, M., 2001. The NCEP–NCAR 50-year reanalysis: monthly means CD-ROM and documentation. Bulletin of the American Meteorological Society 82 (2), 247–267.

Kraus, E.B., Turner, J.S., 1967. A one-dimensional model of the seasonal thermocline: II. The general theory and its consequences. Tellus 19, 98–106.

Lemoine, F., 17 Coauthors, 1997. The development of the NASA GSFC and NIMA joint geopotential model. In: Fujimoto, H. (Ed.), Proceedings of the International Symposium on Gravity, Geoid and MarineGeodesy, IAG Symposium, vol. 117. Springer, Berlin, pp. 461–469.

Lueck, R., Reid, R., 1984. On the production and dissipation of mechanical energy in the ocean. Journal of Geophysical Research 89, 3439–3445.

Mahlman, J.D., Pinto, J.P., Umscheid, L.J., 1994. Transport, radiative, and dynamical effects of the Antarctic ozone hole: a GFDL "SKYHI" model experiment. Journal of the Atmospheric Sciences 51, 489–508.

Munk, W., Wunsch, C., 1998. Abyssal recipes II. Energetics of tidal and wind mixing. Deep-Sea Research I 45, 1977–2010.

Oort, A.H., Anderson, L.A., Peixoto, J.P., 1994. Estimates of the energy cycle of the oceans. Journal of Geophysical Research 99, 7665–7688.

Paparella, F., Young, W.R., 2002. Horizontal convection is non turbulent. Journal of Fluid Mechanics 466, 205–214.

Sandström, J.W., 1908. Dynamische Versuche mit Meerwasser. Annalen der Hydrographie un der Maritimen Meteorologie 36, 6–23.

Sandström, J.W., 1916. Meteorologische Studien im schwedischen Hochgebirge. Goteborgs K. Vetenskaps-och Vitterhetssamhalles Handl., Ser. 4 22 (2) (48pp).

Scott, R.B., 1998. Geostrophic energetics and the small viscosity behavior of an idealized ocean circulation model. Ph.D. Thesis, McGill University, 136pp.

Scott, R.B., 1999. Mechanical energy flux to the surface geostrophic flow using TOPEX/Poseidon data. Physics and Chemistry of the Earth 24 (4), 399–402.

Toggweiler, J.R., Samuels, B., 1995. Effect of Drake passage on the global thermohaline circulation. Deep-Sea Research I 42, 477–500.

Toggweiler, J.R., Samuels, B., 1998. On the ocean's large scale circulation in the limit of no vertical mixing. Journal of Physical Oceanography 28, 1832–1852.

Wang, W., Huang, R.X., 2004a. wind energy input to the surface waves. Journal of Physical Oceanography 34, 1276–1280.

Wang, W., Huang, R.X., 2004b. wind energy input to the Ekman layer. Journal of Physical Oceanography 34, 1267–1275.

Wang, W., Huang, R.X., 2005. An experimental study on thermal circulation driven by horizontal differential heating. Journal of Fluid Mechanics 540, 49–73.

Watanabe, M., Hibiya, T., 2002. Global estimate of the wind-induced energy flux to the inertial motion in the surface mixed layer. Geophysical Research Letters 29 (8), 1239.

Wunsch, C., 1998. The work done by the wind on the oceanic general circulation. Journal of Physical Oceanography 28, 2332–2340.